PROTEIN DESIGN

A designed supramolecular protein assembly with in vivo enzymatic activity

Woon Ju Song and F. Akif Tezcan*

The generation of new enzymatic activities has mainly relied on repurposing the interiors of preexisting protein folds because of the challenge in designing functional, three-dimensional protein structures from first principles. Here we report an artificial metallo-β-lactamase, constructed via the self-assembly of a structurally and functionally unrelated, monomeric redox protein into a tetrameric assembly that possesses catalytic zinc sites in its interfaces. The designed metallo-β-lactamase is functional in the *Escherichia coli* periplasm and enables the bacteria to survive treatment with ampicillin. In vivo screening of libraries has yielded a variant that displays a catalytic proficiency $[(k_{cat}/K_m)/k_{uncat}]$ for ampicillin hydrolysis of 2.3×10^6 and features the emergence of a highly mobile loop near the active site, a key component of natural β-lactamases to enable substrate interactions.

Design and engineering of enzymes not only test our understanding of protein folding and catalysis but can also provide structures and functions that have not been invented by natural evolution [1, 2]. Arguably, the rate-limiting step in both the evolution and rational design of enzymes is the de novo creation of three-dimensional protein architectures through extensive noncovalent interactions. Nature often uses preexisting protein folds, whose active sites can be repurposed for alternative chemistries, as evidenced by the extraordinary functional diversity

Department of Chemistry and Biochemistry, University of California, San Diego, La Jolla, CA 92093-0356, USA.
*Corresponding author. E-mail: tezcan@ucsd.edu

of superfamilies such as the TIM barrel proteins [3] and α/β hydrolases [4]. Similarly, most enzyme design and engineering efforts have had success by using the active sites of preexisting protein structures [5–11] or by exploiting well-established sequence-folding patterns of α-helical bundles [12, 13] for creating new enzymatic functions.

An alternative route is the construction of catalytic sites in newly formed interfaces between proteins or stably folded domains; indeed, interfacial active sites are frequent among natural enzymes [14]. While not benefiting from a preformed scaffold to support an active site, this route is particularly conducive to the introduction of new chemistries, as it is not constrained by the conserved internal structures

of evolved protein folds. The challenge here is that the generation of protein interfaces also requires extensive noncovalent interactions. We [15] and others [16] have shown that construction of new protein interfaces can be aided by coordination by metal ions, which provide large binding energies and have intrinsic chemical properties that can produce nascent enzymatic functions [17]. Kuhlman *et al.* recently reported a designed protein dimer stabilized by interfacial Zn ions that catalyzed the hydrolysis of activated esters in vitro [18]. Nevertheless, the construction of a novel protein fold or quaternary architecture that displays in vivo enzymatic activity has remained an unmet goal, which would represent an important connection between protein design and synthetic biology [19].

Toward this end, we report an artificial, in vivo active metallo-β-lactamase with interfacial catalytic sites, constructed through the metal-directed self-assembly of a monomeric protein. Rapid evolution of β-lactamase activity is the primary mechanism of antibiotic resistance by bacteria [20] and constitutes an appealing and challenging test case for rational protein design and in-lab evolution. The core catalytic motif of metallo-β-lactamases (a nucleophilic, mono- or di-Zn^{II}-OH_2/OH^- species) [21] is, in principle, within facile reach for engineering. Moreover, from a practical viewpoint, β-lactamase activity could be readily screenable in bacterial cells, as it is directly linked to their survival.

Previously, Benkovic *et al.* demonstrated that glyoxalase II could be converted into a metallo-β-lactamase by exchange and engineering of active-site loops, enabled by both enzymes sharing a αβ/βα metallohydrolase fold [5]. To assemble an artificial metallo-β-lactamase with a different architecture, we used as a building block cytochrome cb562 (cyt cb562) [22], a

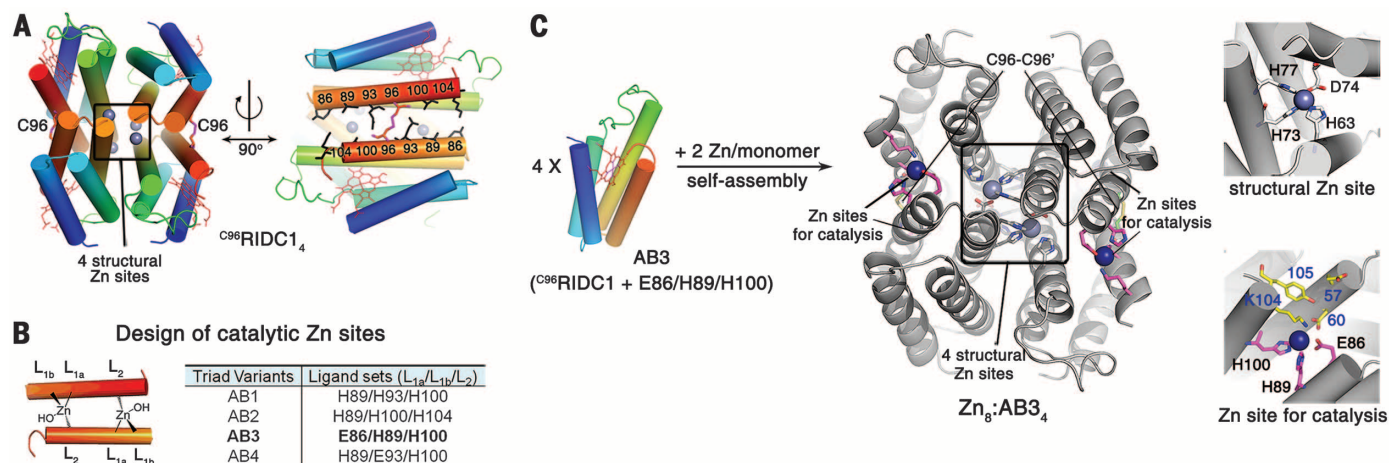**Fig. 1. Structure-guided design of Zn8:AB34.** (**A**) Structure of the tetrameric Zn complex of the self-assembling cyt cb562 variant ^{C96}RIDC14 viewed along one of the three twofold rotational symmetry axes. The four α-helical bundle components are rainbow-colored, red to blue from the C to the N terminus. Residues in the disulfide–cross-linked interfaces used for constructing three-coordinate Zn-anchoring motifs are shown as black sticks. (**B**) List of variants containing triads of Zn-binding residues studied in this work. (**C**) Crystal structure of Zn8:AB34.

four-helix-bundle redox protein that bears no structural, functional, or sequence homology to any metallo-β-lactamase or hydrolytic enzyme. We previously showed that cyt cb_{562} could be converted through a small number of surface mutations into a variant (^{C96}RIDC1) that self-assembles into a D_2 symmetric tetramer through Zn^{II} coordination and a combination of hydrophobic interactions and disulfide bonds (23, 24) (Fig. 1A). A pair of interfaces in this complex (Zn_4:^{C96}RIDC1$_4$) are cross-linked by Cys^{96}-Cys^{96} disulfide bonds. These interfaces present several triads of amino acid positions

that can be used to build the triangular base of a tetrahedral Zn^{II}-OH_2/OH^- coordination motif as a hydrolytic site (Fig. 1, A and B, and table S1). Accordingly, we prepared variants of the ^{C96}RIDC1 monomer (AB1-AB4) with combinations of three coordinating residues (His and/or Glu) appropriately placed such that they would self-assemble into tetramers that possess four structural Zn sites in their interiors and four potentially catalytic Zn sites in their interfaces (Fig. 1C).

We examined the Zn binding capacities and oligomerization properties of the AB variants

by inductively coupled plasma optical emission spectroscopy (ICP-OES) and analytical ultracentrifugation (AUC). All variants except AB2 bound two equivalents of Zn^{II} ions per monomer, equaling eight Zn ions per tetramer, as designed (fig. S1A). Among these, AB3 was the only construct that displayed greater than 90% abundance for a tetrameric species (sedimentation coefficient = 4.5S, fig. S1B) upon Zn binding.

The crystal structure of the Zn complex of AB3 (Zn_8:AB3$_4$), determined at 2.5 Å resolution (Fig. 1C and table S3), confirmed the

Table 1. Summary of hydrolytic activities of the Zn complexes of AB3 variants. The hydrolytic activities were measured in 0.1 M sodium borate buffer (pH 9).

Variants	*p*-Nitrophenyl acetate			Ampicillin				Substrate selectivity (k_{cat}/K_M, ampicillin)/ (k_{cat}/K_M, pNPA)[*‡]
	pK_a	k_{cat} (s^{-1})	k_{cat}/K_M or k_2[*] (s^{-1} M^{-1})	k_{cat} (min^{-1})	k_{cat}/K_M or k_2[*] (min^{-1} M^{-1})	Rate enhancement k_{cat}/k_{uncat}[†]	Catalytic proficiency (k_{cat}/K_M)/k_{uncat}[*†]	
^{A104}AB3	9.0(2)	0.027(8)	32(8)	ND[§]	115(3)[*]	ND[§]	0.7(1) × 10^6	0.06(2)
$^{A104/G57}$AB3	8.9(2)	0.019(4)	29(6)	3.5(8)	350(90)	2.3(6) × 10^4	2.3(0.7) × 10^6	0.20(4)
$^{A104/T105}$AB3	9.2(1)	ND[§]	6.7(7)[*]	ND[§]	100(7)[*]	ND[§]	0.7(1) × 10^6	0.25(3)

[*]In cases where substrate saturation behavior was not observed, a linear fit was used to obtain a second-order rate constant (k_2) instead of k_{cat}/K_M. [†]The background (uncatalyzed) rate constant for ampicillin hydrolysis was measured to be k_{uncat} = 1.5(2) × 10^{-4} min^{-1} [‡]The substrate selectivity was obtained by dividing k_{cat}/K_M or k_2 for ampicillin hydrolysis by that for *p*-nitrophenyl acetate. [§]Cannot be determined owing to lack of substrate saturation behavior.
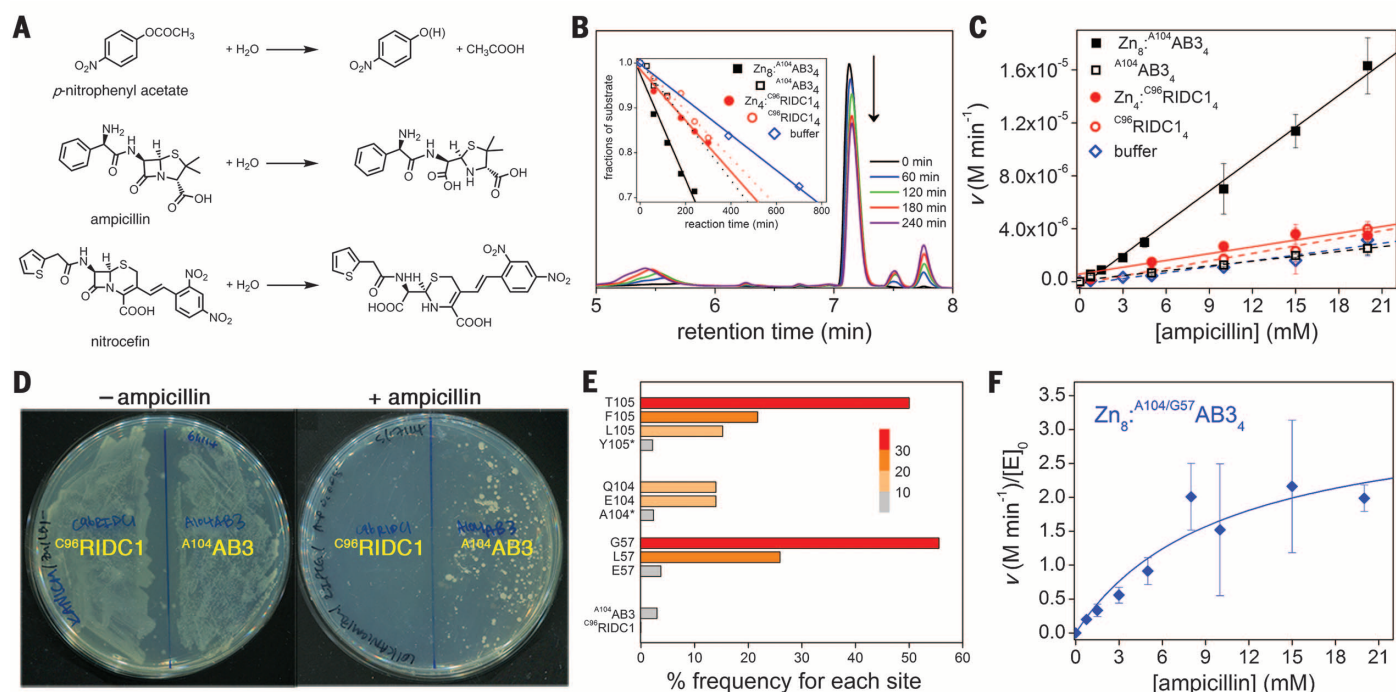

Fig. 2. Investigations of in vitro and in vivo artificial β-lactamase activity. (**A**) Hydrolytic reactions studied in this work. (**B**) A representative set of time-dependent HPLC traces, displaying the consumption of ampicillin through the hydrolytic activity of Zn_8:^{A104}AB3$_4$. (Inset) The plot of fraction of substrate versus reaction time for ^{A104}AB3 and ^{C96}RIDC1 in the presence (closed squares or circles) and absence of Zn (open squares or circles). (**C**) Ampicillin hydrolysis activity of Zn_8:^{A104}AB3$_4$, metal-free ^{A104}AB3$_4$, Zn_4:^{C96}RIDC1$_4$, and metal-free ^{C96}RIDC1$_4$ at var-

ious substrate concentrations. (**D**) Representative LB/agar plates in the absence (left) and presence (right) of ampicillin (0.8 mg/liter). The left and right halves of each plate are streaked with cells expressing ^{C96}RIDC1 and ^{A104}AB3, respectively. (**E**) In vivo survival frequency (percentage of all colonies) of ^{A104}AB3 active-site variants subjected to saturation mutagenesis. Original residues are marked with asterisks. (**F**) Michaelis-Menten kinetics of Zn_8:$^{A104/G57}$AB3$_4$ for ampicillin hydrolysis. Data are mean ± SD.

formation of the desired tetrameric architecture and the two types of Zn coordination geometries. The overall structure of the tetramer is nearly identical to that of the parent Zn_4:$^{C96}RIDC1_4$ (fig. S2A). As designed, each of the four peripheral Zn^{II} ions is anchored by Glu[86] and His[89] side chains from one monomer and His[100] from another. Unexpectedly, the Lys[104] amine group completes the tetrahedral coordination geometry (fig. S2B).

Hydrolytic activity of Zn_8:AB3$_4$ was first evaluated with the chromogenic substrate p-nitrophenyl acetate (pNPA, Fig. 2A). Zn_8:AB3$_4$ displayed no appreciable activity, because the Lys[104] side chain prevents the formation of the Zn^{II}-OH/ OH$_2$ species. However, the K104A mutation yielded a catalytically competent variant, ^{A104}AB3 (fig. S3 and Table 1), which we used for subsequent investigations. Hydrolysis rates by Zn_8:^{A104}AB3$_4$ were measured at pH 9 at different pNPA concentrations, which revealed a Michaelis-Menten behavior with associated kinetic parameters, $k_{cat} = 0.027(8)$ s^{-1} and $k_{cat}/K_M = 32(8)$ s^{-1} M^{-1} (fig. S3A). From the plot of k_{cat}/K_M versus pH, the pK_a value of Zn^{II}-bound H$_2$O was estimated to be 9.0(2) (fig. S3B). At pH = 10, where the tetrameric assembly is largely intact, k_{cat} and k_{cat}/K_M for pNPA hydrolysis were 0.20(5) s^{-1} and 120(20) s^{-1} M^{-1}. These values represent a considerably higher hydrolytic activity relative to synthetic Zn complexes (25) and are in the middle of the range for the most active designed esterases (table S4) (13, 18, 26).

We examined the activity of Zn_8:^{A104}AB3$_4$ for the hydrolysis of ampicillin, a β-lactam antibiotic (Fig. 2A). This was accomplished by high-performance liquid chromatography (HPLC) analysis of the reaction mixture and the characterization of the hydrolysis product by electrospray ionization mass spectrometry (ESI-MS) and nuclear magnetic resonance (NMR) (fig. S4). Zn_8:^{A104}AB3$_4$ hydrolyzed ampicillin (Fig. 2B and Table 1) with a second-order rate constant of $k_2 = 115(3)$ min^{-1} M^{-1} (or 1.92 s^{-1} M^{-1}) at pH 9, but it did not exhibit saturation behavior even at high (20 mM) substrate concentrations, likely due to the lack of appreciable binding interactions with the antibiotic. Ampicillin hydrolysis was considerably slower in the presence of metal-free $^{C96}RIDC1_4$, Zn_4:$^{C96}RIDC1_4$, and metal-free ^{A104}AB3$_4$, at rates near to those observed in a buffer solution (Fig. 2, B and C).

We next asked whether β-lactamase activity of Zn_8:^{A104}AB3$_4$ is also operative within *Escherichia coli* cells and endows them with antibiotic resistance. All cyt cb$_{562}$ variants possess an N-terminal leader sequence, which allows them to be translocated to and mature in the *E. coli* periplasm (22). We previously showed that the periplasm is conducive to the quantitative formation of disulfide-mediated cyt cb$_{562}$ oligomers, which can successfully compete for Zn^{II} binding in that compartment (27). To determine the oligomeric state of ^{A104}AB3 in *E. coli* cells, we extracted the periplasmic contents of the cell pellets via osmotic shock. The extracts were immediately treated with excess iodoacetamide to prevent any uncomplexed ^{A104}AB3 from oligomerizing via disulfide-bond formation after extraction. Size-exclusion chromatography of the extracts revealed that ~70% of ^{A104}AB3 is tetrameric and contained 2.1(2) Zn equivalents per monomer (fig. S5) and negligible levels of other first-row transition metals (Co, Ni, and Cu). Competition titrations of ^{A104}AB3 with the metal-binding indicator MagFura2 (fig. S6 and table S5) confirmed the presence of two distinct types of Zn ions (eight total) with corresponding dissociation constants of 6.7(0.5) nM for one set of four ions and 400(190) nM for the other. These values are comparable to those of natural, periplasmic Zn proteins (28) and explain the quantitative Zn loading of the ^{A104}AB3 tetramers in cells.

To test in vivo β-lactamase activities, we expressed ^{A104}AB3 using kan^+/amp^--pET20b(+) vector in BL21(DE3) *E. coli* cells, which were grown on agar/Luria-Bertani (LB) plates containing various amounts of ampicillin. As a control, we used the $^{C96}RIDC1$ construct, earlier established as having no appreciable β-lactamase activity (Fig. 2, B and C). *E. coli* cells expressing either $^{C96}RIDC1$ or ^{A104}AB3 grew unimpeded on the ampicillin-free LB/agar plates (Fig. 2D). However, only those expressing ^{A104}AB3 survived ampicillin concentrations in the range of 0.8 to 1.1 mg/liter (Fig. 2D), indicating that Zn_8:^{A104}AB3$_4$ has sufficient activity in living cells to serve as a basis for in vivo selection and optimization of catalytic activity.

For the in vivo screening of the synthetic construct, we performed saturation mutagenesis (29) of the four individual amino acid positions that surround the peripheral Zn centers (Glu[57], Asp[60], Lys[104]→Ala, Tyr[105]; Fig. 1C) and thus may form a substrate interaction site. For selection, we fixed the ampicillin concentration in the agar/LB plates at ~1.0 mg/liter and used the frequency of colonies that express a certain AB3 point mutant as a readout for in vivo activity (Fig. 2E). Strains expressing the Gly[57] and Thr[105] point mutants were clear winners, each occurring ~20 times as frequently as the parent Glu[57] and Tyr[105] and about twice as frequently as the second-most-abundant mutants (fig. S8). In contrast, for position 60, the strain with the parent residue (Asp) displayed the highest frequency, and for position 104, no particular mutant dominated over others. Several other factors besides β-lactamase activity of the mutants may affect their survival frequency, such as codon usage, expression levels, and proper assembly. We therefore individually prepared the Zn-mediated assemblies of each variant and determined their in vitro β-lactamase activities (fig. S9). Although there was only a weak correlation between the survival frequencies of the point
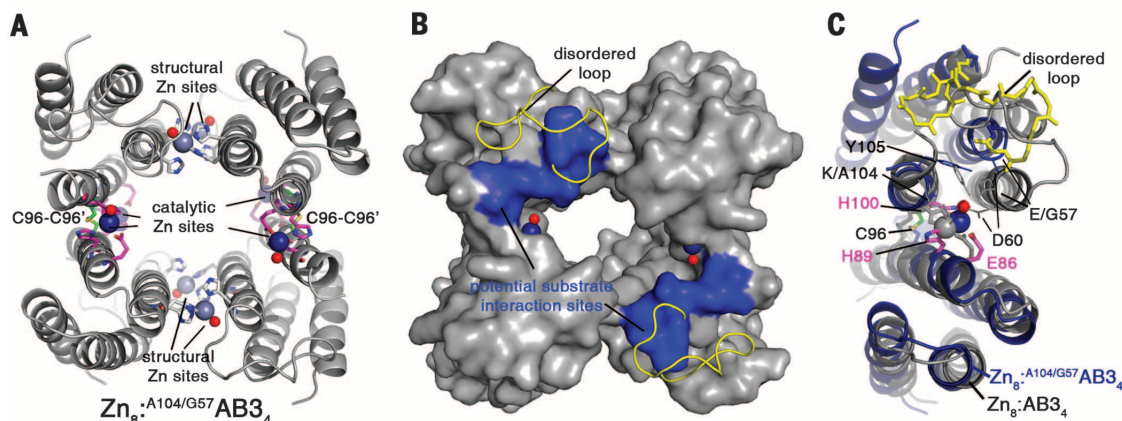

Fig. 3. Crystal structure of Zn_8:$^{A104/G57}$AB3$_4$. (**A**) Cartoon representation of Zn_8:$^{A104/G57}$AB3$_4$. Catalytic and structural Zn ions and the coordinating residues are shown as navy and gray spheres, respectively. The Zn-bound water molecules are shown as red spheres. (**B**) Surface representation of Zn_8:$^{A104/G57}$AB3$_4$. Structurally disordered loops are displayed as yellow ribbons. Potential substrate interaction sites consisting of residues 58 to 60 and 104 to 105 are colored in blue. (**C**) Close-up view of the catalytic Zn sites of Zn_8:$^{A104/G57}$AB3$_4$ (navy) overlaid with Zn_8:AB3$_4$ (gray) structure. Zn-coordinating residues (Glu[86], His[89], and His[100]) and the mobile loop are shown as pink and yellow sticks, respectively.

mutants and their β-lactamase activities, the two variants most frequently represented in in vivo screens, [A104/G57]AB3 and [A104/T105]AB3, were also the most active in vitro.

AUC and Zn-competition titrations indicated that both [A104/G57]AB3 and [A104/T105]AB3 formed Zn-bound tetramers (figs. S10 and S11), with similar binding affinities for Zn as [A104]AB3 (table S5). The pK_a of the Zn^{II}-OH/OH$_2$ active centers was 8.9 for the [A104/G57]AB3 assembly and 9.2 for the [A104/T105]AB3 assembly on the basis of their ampicillin hydrolysis activities (fig. S13 and Table 1). The Zn complex of the [A104/T105]AB3 variant hydrolyzed pNPA with a rate that was ~1/4 of that of [A104]AB3, but its ampicillin hydrolysis activity was essentially the same (Table 1), suggesting that the Y105T mutation may have enhanced interactions with ampicillin. This enhancement was not substantial, however, as the ampicillin hydrolysis rates of the [A104/T105]AB3 variant were linearly dependent on the substrate concentration over the entire concentration range studied (0 to 20 mM) (fig. S14). In contrast, the [A104/G57]AB3 variant hydrolyzed ampicillin more than three times as efficiently as both [A104]AB3 and [A104/T105]AB3 and displayed saturation behavior at increased ampicillin concentrations, with a K_m of 10^{-2} M (Fig. 2F), which is consistent with the emergence of a substrate-binding site. The net rate enhancement (k_{cat}/k_{uncat}) and catalytic proficiency [$(k_{cat}/K_m)/k_{uncat}$] of the Zn_8:[A104/G57]AB3$_4$ complex for ampicillin hydrolysis were 23,000 and 2,300,000, respectively, with an increase in selectivity over pNPA hydrolysis by more than threefold relative to Zn_8:[A104]AB3$_4$ (Table 1).

To examine the formation of a potential ampicillin interaction site and the presence of hydrolytic Zn^{II}-OH/OH$_2$ centers, we determined the structure of Zn_8:[A104/G57]AB3$_4$ at 2.8 Å resolution (Fig. 3 and fig. S15). Unexpectedly, the tetramer displays a substantially more open architecture compared to Zn_8:AB3$_4$ (Fig. 1), ascribed to the elimination of the Lys^{104}-Zn coordination through the K104A mutation. The peripheral Zn sites show the designed coordination to Glu^{86}, His^{89}, and His^{100}, and the Zn-coordinated OH$_2$/OH$^-$ ligand is clearly visible. Although the structural Zn sites of Zn_8:[A104/G57]AB3$_4$ (shown as gray spheres in Fig. 3), which were saturated by protein ligands in the closed Zn_8:[A104]AB3$_4$ architecture (Fig. 1C), are coordinated by only three protein residues and a solvent molecule, they are substantially buried by Arg^{62}, Trp^{41}, and Trp^{66} side chains (fig. S15) and unlikely to be accessible to ampicillin. The opening of the tetrameric architecture is accompanied by the widening of the interfaces containing the catalytic Zn^{II}-OH$_2$/OH$^-$ centers, but the same set of residues (57, 60, 104, 105) remain in position above the Zn^{II}-OH$_2$/OH$^-$ sites as potential substrate interaction sites. Notably, the long, structured loop near the active site, starting from Ala^{43} and terminating in residue 57 is completely disordered because of increased conformational freedom by the E57G mutation and the elimination of the

side-chain interactions of Glu^{57} with Lys^{51} and Ser^{54}. As judged by the packing arrangement of neighboring tetramers in the F222-space-group crystals (65% solvent content), the 43-57 loop is highly mobile and occupies considerable space. Accordingly, binding experiments with 1-anilino-8-naphthalene-sulfonate (1,8-ANS) (fig. S16) suggest that the hydrophobic center of the loop formed by Ala^{43}, Pro^{45}, and Leu^{48} in combination with Met^{58} and Tyr^{105} side chains has become exposed.

The E57G mutation and ensuing loop mobility above the catalytic Zn^{II} centers have potential implications for substrate binding. Molecular docking simulations with ampicillin suggest that the E57G mutation may open up sufficient room for substrate binding and alleviate charge repulsion with the ampicillin carboxylate group to position the β-lactam ring directly above the Zn^{II}-OH/OH$_2$ moiety (fig. S15C). Several possible docking modes orient the ampicillin molecule toward the mobile 43-57 loop and within reach for extensive interactions with the loop. Indeed, Zn_8:[A104/G57]AB3$_4$ can also catalyze the hydrolysis of a bulkier β-lactam, nitrocefin (Fig. 2A), whereas the other variants ([A104]AB3 and [A104/T105]AB3) cannot. Although the catalytic efficiency of Zn_8:[A104/G57]AB3$_4$ for nitrocefin hydrolysis [k_{cat} = 5(1) × 10^{-4} s^{-1}, k_{cat}/K_M = 1.8(6) M^{-1} s^{-1}] (fig. S17) is considerably lower than for ampicillin and the observed rate enhancement (k_{cat}/k_{uncat} ~160-fold) is smaller, the catalytic rate at pH 9 is approximately an order of magnitude higher than that of a known, biomimetic μ-hydroxo-di-Zn^{II} catalyst (30) and comparable to that of a native metallo-β-lactamase, CphA, which possesses a mononuclear Zn^{II}-OH$_2$/OH$^-$ site with pH-independent activity between pH 6 and 9 (31).

In conclusion, we have presented a designed supramolecular protein assembly with in vivo β-lactamase activity, which has allowed its functional screening and optimization via directed evolution. A highly mobile loop near the active site that emerged as an unplanned consequence of in vivo screening is a key feature of natural β-lactamases (32, 33). Our screen was limited to point mutations within a small, nascent active-site pocket. Higher efficiency might be achieved through simultaneous randomization of multiple residues and the enlargement of the active site through loop engineering (34). Moreover, the structural flexibility of the architecture may be used for functional diversification or for engineering allostery (35). Ultimately, Zn_8:[A104/G57]AB3$_4$, a nascent β-lactamase, is only 16 surface mutations away from (i.e., 85% identical to) cyt cb$_{562}$, the parent monomeric redox protein. This illustrates the facility with which protein-protein interfaces nucleated by metal ions lend themselves to creation of new biological structures and functions, whether for rational design or for evolution.

REFERENCES AND NOTES

1. G. Kiss, N. Çelebi-Ölçüm, R. Moretti, D. Baker, K. N. Houk, Angew. Chem. Int. Ed. 52, 5700–5725 (2013).
2. H. Kries, R. Blomberg, D. Hilvert, Curr. Opin. Chem. Biol. 17, 221–228 (2013).
3. R. Sterner, B. Höcker, Chem. Rev. 105, 4038–4055 (2005).
4. M. Nardini, B. W. Dijkstra, Curr. Opin. Struct. Biol. 9, 732–737 (1999).
5. H.-S. Park et al., Science 311, 535–538 (2006).
6. H. K. Privett et al., Proc. Natl. Acad. Sci. U.S.A. 109, 3790–3795 (2012).
7. S. D. Khare et al., Nat. Chem. Biol. 8, 294–300 (2012).
8. L. Giger et al., Nat. Chem. Biol. 9, 494–498 (2013).
9. N. Yeung et al., Nature 462, 1079–1082 (2009).
10. P. S. Coelho, E. M. Brustad, A. Kannan, F. H. Arnold, Science 339, 307–310 (2013).
11. T. K. Hyster, L. Knörr, T. R. Ward, T. Rovis, Science 338, 500–503 (2012).
12. M. Faiella et al., Nat. Chem. Biol. 5, 882–884 (2009).
13. M. L. Zastrow, A. F. Peacock, J. A. Stuckey, V. L. Pecoraro, Nat. Chem. 4, 118–123 (2012).
14. M. H. Ali, B. Imperiali, Bioorg. Med. Chem. 13, 5013–5020 (2005).
15. E. N. Salgado, R. J. Radford, F. A. Tezcan, Acc. Chem. Res. 43, 661–672 (2010).
16. B. S. Der et al., J. Am. Chem. Soc. 134, 375–385 (2012).
17. W. J. Song, P. A. Sontz, X. I. Ambroggio, F. A. Tezcan, Annu. Rev. Biophys 43, 409–431 (2014).
18. B. S. Der, D. R. Edwards, B. Kuhlman, Biochemistry 51, 3933–3940 (2012).
19. K. Channon, E. H. Bromley, D. N. Woolfson, Curr. Opin. Struct. Biol. 18, 491–498 (2008).
20. J. F. Fisher, S. O. Meroueh, S. Mobashery, Chem. Rev. 105, 395–424 (2005).
21. M. W. Crowder, J. Spencer, A. J. Vila, Acc. Chem. Res. 39, 721–728 (2006).
22. J. Faraone-Mennella, F. A. Tezcan, H. B. Gray, J. R. Winkler, Biochemistry 45, 10504–10511 (2006).
23. E. N. Salgado, J. Faraone-Mennella, F. A. Tezcan, J. Am. Chem. Soc. 129, 13374–13375 (2007).
24. J. D. Brodin et al., J. Am. Chem. Soc. 132, 8610–8617 (2010).
25. T. Koike, M. Takamura, E. Kimura, J. Am. Chem. Soc. 116, 8443–8449 (1994).
26. C. M. Rufo et al., Nat. Chem. 6, 303–309 (2014).
27. A. Medina-Morales, A. Perez, J. D. Brodin, F. A. Tezcan, J. Am. Chem. Soc. 135, 12013–12022 (2013).
28. W. Maret, Y. Li, Chem. Rev. 109, 4682–4707 (2009).
29. M. T. Reetz, J. D. Carballeira, Nat. Protoc. 2, 891–903 (2007).
30. N. V. Kaminskaia, C. He, S. J. Lippard, Inorg. Chem. 39, 3365–3373 (2000).
31. M. Vanhove et al., Cell. Mol. Life Sci. 60, 2501–2509 (2003).
32. S. D. B. Scrofan et al., Biochemistry 38, 14507–14514 (1999).
33. P. E. Tomatis et al., Proc. Natl. Acad. Sci. U.S.A. 105, 20605–20610 (2008).
34. D. S. Tawfik, Science 311, 475–476 (2006).
35. N. Tokuriki, D. S. Tawfik, Science 324, 203–207 (2009).

Science
AAAS

A designed supramolecular protein assembly with in vivo enzymatic activity

Woon Ju Song and F. Akif Tezcan